Modeling of polycrystals using a gradient crystal plasticity theory that includes dissipative microstresses

Swantje Bargmann, B. Daya Reddy

Accepted Manuscript

Title: Modeling of polycrystals using a gradient crystal plasticity theory that includes dissipative microstresses

Authors: Swantje Bargmann, B. Daya Reddy

PII: S0997-7538(11)00052-0

DOI: 10.1016/j.euromechsol.2011.04.006

Reference: EJMSOL 2704

To appear in: *European Journal of Mechanics / A Solids*

Received Date: 3 September 2010

Revised Date: 14 April 2011

Accepted Date: 15 April 2011

Please cite this article as: Bargmann, S., Reddy, D. Modeling of polycrystals using a gradient crystal plasticity theory that includes dissipative microstresses, European Journal of Mechanics / A Solids (2011), doi: 10.1016/j.euromechsol.2011.04.006

Modeling of polycrystals using a gradient crystal plasticity theory that includes dissipative microstresses

Swantje Bargmann[a], B. Daya Reddy[c,b]

[a]*Institute of Mechanics, University of Dortmund, Leonhard–Euler-Str. 5, 44227 Dortmund , Germany*
[b]*Department of Mathematics and Applied Mathematics, University of Cape Town, 7701 Rondebosch, South Africa*
[c]*Centre for Research in Computational and Applied Mechanics, University of Cape Town, 7701 Rondebosch, South Africa*

Abstract

This study investigates thermodynamically consistent dissipative hardening in gradient crystal plasticity in a large deformation context. A viscoplastic model which accounts for constitutive dependence on the slip, the slip gradient as well as the slip rate gradient is presented. The model is an extension of that due to Gurtin (Gurtin, M. E., J. Mech. Phys. Solids, 52 (2004) 2545–2568 and Gurtin, M. E., J. Mech. Phys. Solids, 56 (2008) 640–662)), and is guided by the viscoplastic model and algorithm of Ekh et al. (Ekh, M., Grymer, M., Runesson, K. and Svedberg, T., Int. J. Numer. Meths Engng, 72 (2007) 197–220) whose governing equations are equivalent to those of Gurtin for the purely energetic case. In contrast to the Gurtin formulation and in line with that due to Ekh et al., viscoplasticity in the present model is accounted for through a Perzyna-type regularization. The resulting theory includes three different types of hardening: standard isotropic hardening is incorporated as well as energetic hardening driven by the slip gradient. In addition, as a third type, dissipative hardening associated with plastic strain rate gradients is included. Numerical results investigating the different hardening cases are presented.

Keywords: gradient crystal plasticity, dissipative hardening, dual mixed algorithm

1. Introduction

Almost 150 years ago, Tresca [1] was the first to formulate a plasticity theory in a series of papers. The classical theory of plasticity has since undergone steady and significant development, resulting in an elegant set of theories which have served as the basis for numerous theoretical and computational studies (see for example [2, 3]).

It has been recognized for some time that the conventional theories of plasticity are not capable of modeling size effects at the mesoscale such as grain size-dependent hardening in polycrystals or widths of localized shear bands in materials undergoing strain-softening. The influence of the microstructure on the macroscopic material behavior is of particular interest in metallic polycrystals, for example. These are used in automobile or aircraft industries for example, where the optimization of the material properties (not only with respect to the microstructure, of course) is very advanced.

In 1984 Aifantis [4] formulated an extended plasticity theory which has been followed by extensive work on the development of models that account for size effects. These generally have a non-local form, a popular example of which are the strain gradient plasticity models. A non-exhaustive list of theories for strain gradient crystal plasticity theories includes the works of Acharya et al. [5], Bassani [6], Borg [7], Ekh et al. [8], Evers et al. [9], Gurtin [10, 11], respectively Gurtin and Anand [12], Han et al. [13], Kuroda and Tvergaard [14] and Ohno and Okumura [15], for example. Within the context of general gradient plasticity even more publications can be found: see for example the work by Gudmundson [16]. A large number of those are purely energetic, see for example Bargmann et al. [17], Ekh et al. [8], Evers et al. [9, 18], Gurtin [19] and Kuroda and Tvergaard [20], to name just a few. However, the plastically deforming crystal exhibits energetic and dissipative processes. This work is concerned with a gradient crystal plasticity theory that includes energetic and dissipative gradient contributions.

There have been relatively few computational investigations of problems involving strain gradient plasticity. Examples include the works [21, 22, 23, 24] which deal with the Aifantis model. With regard to gradient crystal plasticity, Bittencourt et al. [25] have developed and applied an algorithm for the energetic model of gradient plasticity presented in [19]. In this contribution we rely on the dual mixed finite element algorithm proposed by Svedberg and Runesson [26].

The goal of this work is to formulate and carry out a numerical implemen-

tation of a model of single crystal gradient plasticity that includes dissipative microstresses. The point of departure is the theory due to Gurtin [10, 11]. In this theory microforces are introduced as work-related conjugate quantities to slips and slip gradients; a principle of virtual power then leads to macro- and microforce balance equations. Constitutive equations for plastic flow are developed within a framework that is thermodynamically consistent.

The introduction of a dissipative material length scale is attached to the dissipative microstress. Recently, several works suggesting that within the context of higher-order strain gradient plasticity more than one internal material length scale should be introduced, cf. e.g. Anand et al. [27], Bardella and Giacomini [28], Fleck and Hutchinson [29], Gurtin [30], Lele and Anand [31, 32], Niordson and Legarth [33]. In any case, at a second stage, the material length scales are to be determined by experiments. As noted by Evans and Hutchinson [34], for example, the definitions of these length scales are dependent on the underlying theory. The order of magnitude for an energetic length scale associated with the plastic strain gradient can be estimated based on physical considerations (see e.g. [34, 35]) for some theories. Unfortunately, no such estimate or relation has been presented for a dissipative length scale associated with the plastic slip rate gradient.

Gurtin's theory is one of viscoplasticity. There is a power-law dependence on a generalized plastic strain rate, and no elastic region or yield surface delineates a threshold for plastic flow. In the model developed and considered in this work Gurtin's theory is extended to include the existence of a yield surface depending on the generalized stresses. Furthermore, viscoplasticity is accounted for as a Perzyna-type regularization (see [3] for a summary account) of the flow law. This approach borrows from the work of Ekh et al. [8] who use a Perzyna regularization in the context of a theory that is equivalent to the purely energetic version of Gurtin's theory[1].

The present work is guided further by that of Ekh et al. in that the finite element approximation is of dual-mixed type, in which an independent variable is introduced for the slip gradients. In addition to the modification

[1]Gurtin's microforce balance is also applied by Kuroda and Tvergaard [14], but they only study energetic microforces. Ohno and Okumura [15] incorporated their theory into Gurtin's microforce balance theory studying only energetic contributions. Moreover, Ertürk et al. [36] investigated in detail how the model of Evers et al. [9] can be recast within Gurtin's microforce formulation. The microforce is derived via the physical definition of the Evers-type back stress which plays the main role in their formulation [9].

of Gurtin's original model as described earlier, a further novel feature of the present work lies in the manner in which the dissipative microstress is incorporated into the algorithm. Here, it is treated as an additional variable, together with a corresponding additional flow equation.

The approach taken is that of first formulating the rate-independent theory. This allows for the introduction of the yield function as well as an associative flow law, which play a central role and lead to a constitutive equation for a dissipative microstress $\boldsymbol{\xi}_\alpha^{\text{dis}}$. In a subsequent step the formulation is generalized to viscoplasticity in the spirit of the ideas of Ekh et al. [8], that is, via a Perzyna-type regularization. The approach smoothly unites and extends the ideas of Gurtin and co-workers [30, 11, 32] and Ekh et al. [8], and is essentially a large-deformation counterpart of the rate-independent theory presented and analyzed by Reddy [37].

The rest of this work is structured as follows. Section 2 is devoted to a presentation of the basic kinematics. This is followed in Section 3 by a brief reiteration of the microforce balance equations as set out in [10]. Still following the approach in the last-mentioned work, the free energy and dissipation inequality are introduced in Section 4. The defect part of the free energy depends on the slip gradient $\nabla\gamma_\alpha$, and this leads to the definition of energetic and dissipative microstresses, and a reduced dissipation inequality which forms the basis of the associative flow theory.

The extension to viscoplasticity is presented in Section 5 and the set of equations to be solved is formulated. The theory is implemented into a two-dimensional finite element code as described in Section 6. This is done within the context of a dual-mixed finite element method, similar to that proposed by Ekh et al. [8]. In addition to the displacement $\boldsymbol{u}$, the plastic slip gradient $\nabla\gamma_\alpha$ is modeled as an additional independent field. The fully coupled problem then comprises the global finite element equations for the displacement and slip gradients together with local equations for the slips and dissipative microstresses. Finally, some numerical examples are discussed in Section 7.

2. Kinematics

A solid body B is considered to be a collection of material points. Let $\boldsymbol{X}$ denote the position of a material point in the undeformed and stress-free configuration $\mathcal{B}_0$, the region occupied by the body B at an initial time t_0. Its boundary is denoted by $\partial\mathcal{B}_0$. The body B deforms under the action of

body forces in its domain and surface tractions and prescribed displacements on complementary parts of its boundary. All fields on $\mathcal{B}_0$ are assumed to be continuous and at least once continuously differentiable with respect to position and, in the case of time-dependent problems, also with respect to time t. Moreover, in this work $\mathcal{B}_0$ is assumed not to contain singular surfaces. This assumption is justified because the modeling of material instabilities in materials with microstructure and possessing internal length scales in this work results in diffuse rather than sharp interfaces between homogeneous regions in $\mathcal{B}_0$.

The motion of the reference configuration $\mathcal{B}_0$ is described by the vector-valued function

$$\boldsymbol{\varphi} : \mathcal{B}_0 \times \mathbb{R}_+ \to \mathcal{B}_t \ \text{ with } \boldsymbol{\varphi}(\boldsymbol{X}, t) := \boldsymbol{\varphi}_t(\boldsymbol{X}) = \boldsymbol{x}, \tag{1}$$

where $\boldsymbol{x}$ denotes the position of the material point $\boldsymbol{X}$ in the deformed (spatial) configuration $\mathcal{B}_t$ at time t. As usual, the motion $\boldsymbol{\varphi}_t$ is assumed to be one-to-one, continuously differentiable, and with a continuous inverse. That is, $\boldsymbol{\varphi}_t$ is required to be a diffeomorphism.

The deformation gradient $\boldsymbol{F}$ is defined by

$$\boldsymbol{F} : \mathcal{T}\mathcal{B}_0 \to \mathcal{T}\mathcal{B}_t \ \text{ with } \ \boldsymbol{F} := \nabla \boldsymbol{\varphi}_t(\boldsymbol{X}) \tag{2}$$

where $\mathcal{T}\mathcal{B}_0$ and $\mathcal{T}\mathcal{B}_t$ are respectively the tangent spaces at $\boldsymbol{X}$ and $\boldsymbol{x}$, and ∇ denotes the gradient operator with respect to $\boldsymbol{X}$.

In large-strain plasticity it is assumed that the deformation gradient may be decomposed multiplicatively into an elastic part $\boldsymbol{F}^{\mathrm{e}}$ and a plastic part $\boldsymbol{F}^{\mathrm{p}}$, that is,

$$\boldsymbol{F} = \boldsymbol{F}^{\mathrm{e}} \cdot \boldsymbol{F}^{\mathrm{p}}. \tag{3}$$

The plastic part $\boldsymbol{F}^{\mathrm{p}}$ describes the deformation from the tangent space $\mathcal{T}\mathcal{B}_0$ to the intermediate tangent space $\mathcal{T}\bar{\mathcal{B}}$ associated with the intermediate configuration. The plastic part of the deformation gradient arises due to inelastic slip along the preferred crystal planes, while the elastic contribution $\boldsymbol{F}^{\mathrm{e}}$ accounts for reversible lattice distortion and rotation.

The Green–Lagrange strain $\boldsymbol{E}$ is defined by

$$\boldsymbol{E} := \frac{1}{2}[\boldsymbol{F}^t \cdot \boldsymbol{F} - \boldsymbol{I}] \tag{4}$$

and the corresponding strain quantity associated with $\boldsymbol{F}^e$ is defined by

$$\boldsymbol{E}^{\mathrm{e}} := \frac{1}{2}[[\boldsymbol{F}^{\mathrm{e}}]^t \cdot \boldsymbol{F}^{\mathrm{e}} - \bar{\boldsymbol{I}}]. \tag{5}$$

In crystal plasticity slip takes place on specified planes and in directions that are specified with respect to the intermediate configuration. The slip direction and unit normal to the plane corresponding to the slip system α are denoted respectively by $\boldsymbol{s}_\alpha$ and $\boldsymbol{n}_\alpha$ while γ_α represents the corresponding scalar-valued plastic slip field. For convenience the current formulation is restricted to quasi-static, isothermal processes.

Following Rice [38], the evolution of plastic deformation is described by a kinematic relation in which the plastic velocity gradient tensor $\boldsymbol{L}^{\mathrm{p}}$ is given by

$$\boldsymbol{L}^{\mathrm{p}} = \dot{\boldsymbol{F}}^{\mathrm{p}} \cdot [\boldsymbol{F}^{p}]^{-1} = \sum_{\alpha} \dot{\gamma}_\alpha [\boldsymbol{s}_\alpha \otimes \boldsymbol{n}_\alpha]. \tag{6}$$

Here and henceforth summation is over all slip systems. The criterion for plastic slip on a plane depends inter alia on the magnitude of the resolved shear stress or Schmid stress τ_α, which is given by

$$\tau_\alpha = \boldsymbol{s}_\alpha \cdot \boldsymbol{M} \cdot \boldsymbol{n}_\alpha, \tag{7}$$

with $\boldsymbol{M}$ being the Mandel stress

$$\boldsymbol{M} = \boldsymbol{F}^{\mathrm{e}} \cdot \frac{\partial \boldsymbol{\Psi}^{\mathrm{e}}}{\partial \boldsymbol{F}^{\mathrm{e}}}. \tag{8}$$

3. Force balances

The macroscopic problem is governed by the balance of momentum, here stated in its quasi-static form

$$\mathrm{Div}\boldsymbol{P} + \boldsymbol{b} = \boldsymbol{0}, \tag{9}$$

with $\boldsymbol{P}$ and $\boldsymbol{b}$ denoting respectively the first Piola–Kirchhoff stress tensor and the body force. Along with the momentum balance (9) goes the traction condition

$$\boldsymbol{t}(\boldsymbol{N}) := \boldsymbol{P} \cdot \boldsymbol{N}, \tag{10}$$

where $\boldsymbol{t}$ denotes the macroscopic traction vector and $\boldsymbol{N}$ is the macroscopic outward unit normal vector on a surface in the material configuration.

At the microlevel, the approach due to Gurtin (see for example [10, 11]) is followed: specifically, a scalar microforce π_α and vector microstress $\boldsymbol{\xi}_\alpha$ work-conjugate to slip-rate $\dot{\gamma}_\alpha$ and slip-rate gradient $\nabla\dot{\gamma}_\alpha$ respectively are

introduced, together with a surface microtraction χ_α conjugate to $\dot{\gamma}_\alpha$. The microscopic virtual power relation leads to the microscopic force balance

$$\operatorname{Div} \boldsymbol{\xi}_\alpha + \tau_\alpha - \pi_\alpha = 0, \tag{11}$$

The microforce balance (11) has to hold for every slip system α. The micro- and the macrolevel are coupled via the Schmid stress τ_α, i.e. Eq. (7). In the case of a purely elastic deformation Eq. (11) reduces to the relation $\pi_\alpha = \tau_\alpha$.

In analogy to Eq. (10), a microscopic traction condition is defined on the crystal boundaries by

$$\chi_\alpha(\boldsymbol{N}) := \boldsymbol{\xi}_\alpha \cdot \boldsymbol{N}, \tag{12}$$

with χ_α denoting the microscopic traction.

Boundary conditions need to specified to accompany the microforce balance equation. There exist two very commonly used kinds: the micro-hard boundary condition

$$\gamma_\alpha = 0 \quad \text{on} \quad \partial\mathcal{B}_{0H} \tag{13}$$

and the micro-free condition

$$\boldsymbol{\xi}_\alpha \cdot \boldsymbol{N} = 0 \quad \text{on} \quad \partial\mathcal{B}_{0F} \tag{14}$$

where $\partial\mathcal{B}_{0F}$ and $\partial\mathcal{B}_{0H}$ are complementary parts of the boundary $\partial\mathcal{B}_0$. The micro-hard boundary conditions assume that the plastic slip vanishes on the boundary, i.e. dislocations are not able to penetrate the grain boundaries. On the other hand, micro-free conditions assume stress-free boundaries, i.e. that the micro-stress $\boldsymbol{\xi}_\alpha$ vanishes there. For a third (more advanced but more complex) option which takes into account the degree of mismatch between the slip systems of neighboring grains, the reader is referred to [39].

4. The free energy

We assume the existence of a free energy Ψ per unit reference volume which depends on the elastic deformation and the slip gradients $\nabla\gamma_\alpha$. The free energy is assumed to be decomposed additively into elastic and defect contributions; that is,

$$\Psi = \Psi^{\mathrm{e}}(\boldsymbol{E}^{\mathrm{e}}) + \Psi^{\mathrm{d}}(\{\nabla\gamma_\alpha\}) \tag{15}$$

where each of the components is quadratic in its arguments. In particular the elastic part Ψ^{e} has the standard St. Venant form

$$\Psi^{\mathrm{e}}(\boldsymbol{E}^{\mathrm{e}}) = \frac{\lambda}{2}\left[\mathrm{tr}\boldsymbol{E}^{\mathrm{e}}\right]^2 + \mu \mathrm{tr}\left([\boldsymbol{E}^{\mathrm{e}}]^2\right), \tag{16}$$

with λ and μ being the Lamé parameters, while the defect term is given by

$$\Psi^{\mathrm{d}}(\{\nabla\gamma_\alpha\}) = \frac{1}{2}\sum_\alpha l_\alpha^2 \nabla\gamma_\alpha \cdot \boldsymbol{H}_\alpha^g \cdot \nabla\gamma_\alpha\,, \tag{17}$$

where $\boldsymbol{H}_\alpha^g = H_\alpha^g \boldsymbol{s}_\alpha \otimes \boldsymbol{s}_\alpha$ is a tensor of defect moduli and ℓ_α is a material parameter corresponding to a length scale, in both cases specified for each slip system.

The free energy imbalance is used to guide the construction of a set of constitutive relations for elastic behavior and plastic flow. It takes the form

$$\dot{\Psi} - [\boldsymbol{F}\cdot\boldsymbol{P}] : \dot{\boldsymbol{E}}^{\mathrm{e}} - \sum_\alpha \left[\pi_\alpha \dot{\gamma}_\alpha + \boldsymbol{\xi}_\alpha \cdot \nabla\dot{\gamma}_\alpha\right] \leq 0 \tag{18}$$

(cf. the arguments by Gurtin [10]). Substitution of Eqs. (15) and (16) in this inequality leads, after the usual arguments, to the elastic law

$$\boldsymbol{F}\cdot\boldsymbol{P} = \boldsymbol{F}\cdot\frac{\partial\Psi^{\mathrm{e}}}{\partial\boldsymbol{F}} = \lambda \mathrm{tr}\,\boldsymbol{E}^e + 2\mu\boldsymbol{E}^e \tag{19}$$

and the reduced dissipation inequality

$$\sum_\alpha \left[\pi_\alpha\dot{\gamma}_\alpha + (\boldsymbol{\xi}_\alpha - \boldsymbol{\xi}_\alpha^{\mathrm{en}})\cdot\nabla\dot{\gamma}_\alpha\right] \geq 0 \tag{20}$$

where

$$\boldsymbol{\xi}_\alpha^{\mathrm{en}} \;:=\; \frac{\partial\Psi^{\mathrm{d}}}{\partial\nabla\gamma_\alpha} = l_\alpha^2 \boldsymbol{H}_\alpha^g \cdot \nabla\gamma_\alpha \tag{21}$$

is the energetic component of the internal microstress. The microstress $\boldsymbol{\xi}$ may be decomposed additively into energetic and dissipative components $\boldsymbol{\xi}^{\mathrm{en}}$ and $\boldsymbol{\xi}^{\mathrm{dis}}$, so that

$$\boldsymbol{\xi}_\alpha^{\mathrm{dis}} \;:=\; \boldsymbol{\xi}_\alpha - \boldsymbol{\xi}_\alpha^{\mathrm{en}} \tag{22}$$

(see for example Gurtin [11] in the context of single crystal plasticity or Anand et al. [27] and Lele and Anand [31, 32] in the context of isotropic materials).

Using this definition, the reduced dissipation inequality (20) becomes

$$\sum_{\alpha} \left[\pi_\alpha \dot{\gamma}_\alpha + \boldsymbol{\xi}_\alpha^{\mathrm{dis}} \cdot \nabla \dot{\gamma}_\alpha \right] \geq 0 \,. \tag{23}$$

Elastic region and yield function.

We begin the formulation of the flow law within a rate-independent context, and later generalize to the case of viscoplasticity (see [37] for a corresponding development in the context of small strains).

Guided by the reduced dissipation inequality, i.e. Eq. (23), we define the generalized stress

$$\mathsf{S}_\alpha = \begin{pmatrix} \pi_\alpha \\ l_{d(\alpha)}^{-1} \boldsymbol{\xi}_\alpha^{\mathrm{dis}} \end{pmatrix} \tag{24}$$

where $l_{d(\alpha)}$ is a dissipative length scale[2] which may vary for each slip system, and the elastic region on the α th slip plane by

$$\Phi(\mathsf{S}_\alpha) = |\mathsf{S}_\alpha| - [Y_\alpha + \kappa_\alpha] \leq 0 \,. \tag{25}$$

Here Y_α is the initial yield stress on the αth slip plane and κ_α the hardening stress. Furthermore,

$$|\mathsf{S}_\alpha| = \left[|\pi_\alpha|^2 + l_{d(\alpha)}^{-2} |\boldsymbol{\xi}_\alpha^{\mathrm{dis}}|^2 \right]^{1/2} . \tag{26}$$

Assuming a normality law we have

$$\begin{aligned} \dot{\gamma}_\alpha &= \dot{\lambda}_\alpha \frac{\partial \Phi_\alpha}{\partial \pi_\alpha} = \dot{\lambda}_\alpha \frac{\pi_\alpha}{|\mathsf{S}_\alpha|} \,, \\ \nabla \dot{\gamma}_\alpha &= \dot{\lambda}_\alpha \frac{\partial \Phi_\alpha}{\partial \boldsymbol{\xi}_\alpha^{\mathrm{dis}}} = \dot{\lambda}_\alpha \frac{l_{d(\alpha)}^{-2} \boldsymbol{\xi}_\alpha^{\mathrm{dis}}}{|\mathsf{S}_\alpha|} \,, \end{aligned} \tag{27}$$

where $\dot{\lambda}_\alpha \geq 0$ is a scalar multiplier, together with the complementarity conditions

$$\Phi_\alpha \leq 0 \,, \quad \dot{\lambda}_\alpha \geq 0 \,, \quad \dot{\lambda}_\alpha \Phi_\alpha = 0 \,. \tag{28}$$

[2]Material length scales which are connected to strain rate gradients can also be found in the contributions of e.g. Aifantis [4], Bardella and Giacomini [28], Fleck and Hutchinson [29], Lele and Anand [31, 32], Niordson and Legarth [33], Voyiadjis and Deliktas [40].

At flow, when $\Phi_\alpha = 0$, we have $|\mathsf{S}_\alpha| = Y_\alpha + \kappa_\alpha$ and

$$\left[(\dot{\gamma}_\alpha)^2 + l_{d(\alpha)}^2 |\nabla\dot{\gamma}_\alpha|^2\right]^{1/2} = \dot{\lambda}_\alpha := d_\alpha \tag{29}$$

where d_α is the effective flow rate associated with the αth slip surface. It is thus convenient to define a generalized strain measure

$$\Gamma_\alpha = \begin{pmatrix} \gamma_\alpha \\ l_{d(\alpha)}\nabla\gamma_\alpha \end{pmatrix} \tag{30}$$

so that

$$|\dot{\Gamma}_\alpha| = d_\alpha \,. \tag{31}$$

In the case of plastic flow equations (27) may be inverted to give

$$\begin{aligned} \pi_\alpha &= \frac{|\mathsf{S}_\alpha|}{d_\alpha}\dot{\gamma}_\alpha \,, \\ \boldsymbol{\xi}_\alpha^{\mathrm{dis}} &= \frac{|\mathsf{S}_\alpha|}{d_\alpha} l_{d(\alpha)}^2 \nabla\dot{\gamma}_\alpha \,. \end{aligned} \tag{32}$$

For convenience linear isotropic hardening is assumed, so that

$$\kappa_\alpha := H_\alpha^l k_\alpha \tag{33}$$

where k_α is the equivalent plastic strain on the αth slip system, defined by

$$\dot{k}_\alpha := \dot{\lambda}_\alpha = d_\alpha \tag{34}$$

and H_α^l is the local hardening modulus, i.e. a positive material constant. This definition is a natural extension of the approach by Ekh et al. [8], where $\dot{k}_\alpha = \dot{\gamma}_\alpha$ was used. Furthermore, it leads to a consistent model in this contribution.

The approach of Ekh et al. [8] differs from that of Gurtin and co-authors and thus from what is described above. Ekh et al. [8] derive a microstress, here denoted by $\kappa_{\mathrm{Ekh}\,\alpha}$, via the second law of thermodynamics. The microstress is defined through the free energy Ψ which in addition to the gradient contribution stated in Eq. (17) depends quadratically on the plastic slip $\{\gamma_\alpha\}$. Moreover, it is split up additively into local and gradient hardening contributions in the form

$$\begin{aligned} \kappa_{\mathrm{Ekh}\,\alpha} &:= \kappa_{\alpha,l} + \kappa_{\alpha,g} \\ &:= \frac{\partial\Psi}{\partial\gamma_\alpha} - \mathrm{Div}\left(\frac{\partial\Psi}{\partial\nabla\gamma_\alpha}\right) \quad \text{in } \mathcal{B}_{0,\,\mathrm{grain}},\ \alpha = 1, 2, ..., n_{\mathrm{slip}} \end{aligned} \tag{35}$$

where $\mathcal{B}_{0,\,\mathrm{grain}}$ denotes the material domain associated with a grain. As stated in Bargmann et al. [41], the gradient contribution of the microstress can be identified with the divergence of the energetic microforce of Gurtin: that is, $\kappa_{\alpha,g}$ corresponds to $\mathrm{Div}\,\boldsymbol{\xi}_\alpha^{\mathrm{en}}$. Both play the role of an energetic backstress. Moreover, in case of pure energetic hardening, the hardening stresses stated in Eqs. (33) and (35) are equivalent.

Isotropic hardening, while dissipative in nature, can be equivalently characterized by a non-recoverable defect energy, as shown by Gurtin and Reddy [42]. The defect energy Ψ^{d} may then be defined as a function of the equivalent plastic strain k_α by

$$\Psi^{\mathrm{d}}(\{k_\alpha\}) = \frac{1}{2}\sum_\alpha H_\alpha^l k_\alpha^2\,. \tag{36}$$

The thermodynamic force conjugate to the equivalent plastic strain k_α is given by $g_\alpha := -\kappa_\alpha$, so that

$$g_\alpha = \frac{\partial \Psi^{\mathrm{d}}}{\partial k_\alpha} = -H_\alpha^l k_\alpha\,. \tag{37}$$

With this definition, by following the steps leading to Eq. (23) it is seen that the reduced dissipation inequality becomes

$$\sum_\alpha \left[\pi_\alpha \dot{\gamma}_\alpha + \boldsymbol{\xi}_\alpha^{\mathrm{dis}} \cdot \nabla \dot{\gamma}_\alpha + g_\alpha \dot{k}_\alpha\right] \geq 0\,. \tag{38}$$

This suggests the definition of the yield function Φ as a function of the generalized stress S_α and g_α; that is, Eq. (25) becomes

$$\Phi = \overline{\Phi}(\mathsf{S}_\alpha, g_\alpha) = |\mathsf{S}_\alpha| - [Y_\alpha - g_\alpha] \leq 0\,.$$

It then follows from the associative flow rule that

$$\begin{aligned} \dot{\Gamma}_\alpha &= \dot{\lambda}_\alpha \frac{\mathsf{S}_\alpha}{|\mathsf{S}_\alpha|}\,, \\ \dot{k}_\alpha &= \dot{\lambda}_\alpha \frac{\partial \overline{\Phi}}{\partial g_\alpha} = \dot{\lambda}_\alpha\,, \end{aligned} \tag{39}$$

the second equation reproducing relation (34).

The formulation presented here is a rate-independent one that is based on the Gurtin-type approach. Some key distinctions are worth noting:

(i) The notion of an elastic region, yield function and normality law are explicitly introduced in the present formulation. These in turn are defined on the basis of the structure of the reduced dissipation inequality.

(ii) Local hardening is captured via the hardening law in a conventional way, while non-local effects appear through the inclusion of the microstress in the microforce balance and through the defect term in the free energy.

Both approaches necessitate the existence of microscopic boundary conditions.

5. A viscoplastic model with dissipative microstress

In this section the constitutive equations for plastic flow are generalized to the case of viscoplasticity. In the works of Gurtin, Anand and coworkers (see for example [10, 11, 12, 31, 32]), viscoplastic regularization entails extensions of Eq. (32) which take the form

$$\begin{array}{rcl} \pi & \propto & \mathcal{S}R(d_\alpha)\dot{\gamma}_\alpha \\ \boldsymbol{\xi}^{\mathrm{dis}} & \propto & \mathcal{S}R(d_\alpha)\nabla\dot{\gamma}_\alpha \end{array} \tag{40}$$

where $R(d_\alpha) = [d_\alpha/d_0]^q$, d_0 is a reference generalized strain rate, and q is a positive real exponent. Furthermore $\mathcal{S}$ denotes the positive-valued flow resistance. This is also the approach taken by other authors such as Evers et al. [9]. It follows that in these approaches the dissipative microstress $\boldsymbol{\xi}^{\mathrm{dis}}$ is defined via Eq. $(40)_2$. However, the approach by these authors does not allow for elastic behavior, for the case in which the generalized stress lies in the elastic region.

The approach to viscoplastic regularization taken in this work differs from that just described. Here the goal is to extend the approach of Ekh et al. [8] by introducing a regularization of Perzyna type: in the case of a solely energetic microstress, as in [8], which can be obtained by setting $l_{d(\alpha)} = 0$ in the set of equations in the previous section, the flow law

$$\dot{\gamma}_\alpha = \dot{\lambda}_\alpha \operatorname{sgn} \pi_\alpha \tag{41}$$

becomes

$$\dot{\gamma}_\alpha = \frac{1}{t_{\star,\alpha}} \langle \Phi_\alpha \rangle^m \operatorname{sgn} \pi_\alpha \tag{42}$$

or equivalently

$$\dot{\lambda}_\alpha = \frac{1}{t_{\star,\alpha}} \langle \Phi_\alpha \rangle^m \,, \tag{43}$$

where

$$\langle x \rangle := \frac{1}{2}[x + |x|]$$

and where $t_\star$ is a relaxation time and m the rate sensitivity parameter. Moreover, the restriction on the sign of the yield function Φ_α, i.e. Eq. $(28)_1$, does not hold any longer, of course. In other words, the yield function Φ_α can be positive, negative or zero.

In the present approach the elastic region is defined by $\Phi_\alpha < 0$ and the plastic by $\Phi_\alpha \geq 0$. The objective in this work is to extend this approach to the case of dissipative microstresses in a manner that is amenable to computational implementation.

Thus the viscoplastic flow law is defined by

$$\dot{\Gamma}_\alpha = \frac{1}{t_{\star,\alpha}} \langle \Phi_\alpha \rangle^m \frac{\mathsf{S}_\alpha}{|\mathsf{S}_\alpha|}. \tag{44}$$

From Eqs. (31) and (44) it follows that

$$|\dot{\Gamma}_\alpha| = d_\alpha = \frac{1}{t_{\star,\alpha}} \langle \Phi_\alpha \rangle^m \,. \tag{45}$$

In the case of flow, that is, when $\Phi_\alpha > 0$, equation (45) is equivalent to

$$|\mathsf{S}_\alpha| = (t_{\star,\alpha} d_\alpha)^{1/m} + Y_\alpha + \kappa_\alpha, \tag{46}$$

where local hardening enters via the last term on the right-hand side. Thus from Eqs. (44) and (45) it follows that

$$\dot{\Gamma}_\alpha = \left[\frac{d_\alpha}{(t_{\star,\alpha} d_\alpha)^{1/m} + Y_\alpha + \kappa_\alpha} \right] \mathsf{S}_\alpha \tag{47}$$

or, in component form,

$$\dot{\gamma}_\alpha = \left[\frac{d_\alpha}{(t_{\star,\alpha} d_\alpha)^{1/m} + Y_\alpha + \kappa_\alpha} \right] \pi_\alpha \,, \tag{48}$$

$$\nabla \dot{\gamma}_\alpha = \left[\frac{d_\alpha}{(t_{\star,\alpha} d_\alpha)^{1/m} + Y_\alpha + \kappa_\alpha} l_{d(\alpha)}^{-2} \right] \boldsymbol{\xi}_\alpha^{\mathrm{dis}} \,. \tag{49}$$

The next step is to eliminate the dissipative microstress $\boldsymbol{\xi}_\alpha^{\text{dis}}$ from these equations.

Substitution in Eq. (48) for the internal microforce π_α using the microforce balance equation (11) leads to the non-local flow rule

$$\dot{\gamma}_\alpha = \frac{d_\alpha}{(t_{\star,\alpha} d_\alpha)^{1/m} + Y_\alpha + \kappa_\alpha} \left[\tau_\alpha + \operatorname{Div} \boldsymbol{\xi}_\alpha^{\text{en}} + \operatorname{Div} \boldsymbol{\xi}_\alpha^{\text{dis}} \right]. \tag{50}$$

An explicit expression for the dissipative microstress[3] $\boldsymbol{\xi}_\alpha^{\text{dis}}$ is obtained by inverting (49), which gives

$$\boldsymbol{\xi}_\alpha^{\text{dis}} = \frac{(t_{\star,\alpha} d_\alpha)^{1/m} + Y_\alpha + \kappa_\alpha}{d_\alpha} l_{d(\alpha)}^2 \nabla \dot{\gamma}_\alpha, \tag{51}$$

showing the dependence of the dissipative microstress $\boldsymbol{\xi}_\alpha^{\text{dis}}$ on the plastic slip rate gradient $\nabla \dot{\gamma}_\alpha$. This dependence is highly non-linear because d_α depends on the slip rate gradient $\nabla \dot{\gamma}_\alpha$ as well. A similar expression for dissipative hardening, being linear in the plastic slip rate gradient $\nabla \dot{\gamma}_\alpha$ has been derived by Anand et al. [27], Fredriksson and Gudmundson [43] and Lele and Anand [31, 32] for isotropic materials and in the contribution of Gurtin [11] for single crystal plasticity (see also Remark below).

Finally, the use of Eq. (51) and the expression (21) for the energetic microstress $\boldsymbol{\xi}_\alpha^{\text{en}}$ in Eq. (50) leads to an expression for the plastic slip rate that is entirely in terms of $\nabla \dot{\gamma}_\alpha$, d_α, and the hardening variable $\kappa_{\alpha,l}$. It is worth noting that in this contribution the regularization is introduced from the start via the evolution equation (44). Then, in turn, the relation between the dissipative microstress $\boldsymbol{\xi}_\alpha^{\text{dis}}$ and the slip rate gradient $\nabla \dot{\gamma}_\alpha$ is a derived result (see Eq. (51)) and not a definition.

In the case of purely energetic microstress, that is, for $l_{d(\alpha)} = 0$, the evolution equation (44) reduces to the flow law

$$\dot{\gamma}_\alpha = \frac{1}{t_{\star,\alpha}} \langle \Phi_\alpha \rangle^m, \tag{52}$$

which is the expression used in Ekh et al. [8]. For the dissipative case, for which $l_{d(\alpha)} \neq 0$, the generalization captured in Eqs. (44)-(51) essentially follows from the dissipation inequality in the form (23).

[3]Since the scalar d_α is not constant, this gives rise to an additional complexity in terms of the divergence term $\operatorname{Div} \boldsymbol{\xi}_\alpha^{\text{dis}}$.

6. Finite element algorithm

The finite element algorithm used for our computations is similar to the dual mixed framework[4] of Ekh et al. [8]. As in that work, the governing equations are discretized using the Bubnov–Galerkin finite element method in space. The problem is also discretized in time with time derivatives approximated by an Euler backward difference. In addition to the two governing equations (9) and (50) a dual variable $\boldsymbol{g}_\alpha$ defined by

$$\boldsymbol{g}_\alpha := \nabla\gamma_\alpha. \tag{53}$$

is introduced in each slip system. This definition differs from that in the algorithm proposed by Ekh et al. [8] who define and use the scalar directional gradient $g_\alpha := \nabla\gamma_\alpha \cdot \boldsymbol{s}_\alpha$. In line with Ekh et al. [8], the balance of momentum (9) and the gradient equation (53) are solved globally and monolithically with a Newton–Raphson scheme to account for the non-linearities. The second order partial differential equation (50), that is, the flow rule, is solved locally in each element. Due to the non-linearities, Newton–Raphson iterations are required here as well.

The macro-domain $\mathcal{B}_0$ represents a polycrystal assembly consisting of a collection of grains. The domain of such a grain is denoted by $\mathcal{B}_{0,\text{grain}}$ and its boundary by $\partial\mathcal{B}_{0,\text{grain}}$. The task is then to find the displacement $\boldsymbol{u}$ and slips γ_α in each grain which satisfy the governing equations inside each grain together with the boundary conditions on the grain boundaries and the boundary of the macro-domain $\mathcal{B}_0$.

The model is implemented in a two-dimensional code and plane strain is assumed throughout. Microhard boundary conditions are assumed so that

$$\gamma_\alpha = 0 \qquad \text{on } \partial\mathcal{B}_{0,\text{grain}}, \tag{54}$$

see also end of Section 3. Our choice is motivated by the statement in e.g. Gurtin and Needleman [45]: "When the theory is generalized to allow each of the microstress $\boldsymbol{\xi}_\alpha$ to have a dissipative contribution on the slip-gradient rates, then the hard slip conditions are appropriate.".

The introduction of the independent variable $\boldsymbol{g}_\alpha$ and the use of a mixed approach has a significant benefit. By using a mixed approach it is possible

[4]Similar approaches which, as in this contribution, treat quantities of the gradient type as primary variables include [9, 14, 44].

to construct a two-stage algorithm in which in the first stage the displacement and the mixed variable are obtained, while in the second stage the slip increments can be solved for locally. Furthermore, the staggered approach is possible using simple approximations of the variables, for example linear approximations for displacement and slip gradient $\boldsymbol{g}_\alpha$, and piecewise-constant approximations for the slips $\{\gamma_\alpha\}$ on triangular elements.

Generally, one can choose the set of finite element approximations such that the displacement $\boldsymbol{u}$ and gradient $\boldsymbol{g}_\alpha$ are of the same degree and the slips γ_α one order less.

There exist different model assumptions on "geometric constraints" which infer restrictions on the displacement $\boldsymbol{u}$. Relaxed Taylor assumptions are applied: that is, the displacements are prescribed at the boundaries and not inside the grains.

The algorithm is summarized in Box 1.

Box 1: Algorithm for dual mixed finite element method

1. Assume given values for the nodal displacement vector $\boldsymbol{u}^{(k)}$, the nodal vector of the gradient $\boldsymbol{g}_\alpha := \nabla\gamma_\alpha$, i.e. $\underline{\boldsymbol{g}}^{(k)}$, and (converged) values $\Delta\boldsymbol{\gamma}^{(k)}$ at time k.

2. "Grain boundary iteration loop": Solve the quasi-static balance of momentum (resulting from Eq. (9)) for the nodal displacement vector $\boldsymbol{u}_{\mathrm{gb}}^{(k+1)}$ on the grain boundaries[a].

a. "Inner grain iteration loop": Given the nodal displacements $\boldsymbol{u}_{\mathrm{gb}}^{(k+1)}$ on the grain boundaries, solve the quasi-static balance of momentum and the gradient equation $\boldsymbol{g}_\alpha - \nabla\gamma_\alpha = \boldsymbol{0}$ for the displacements $\boldsymbol{u}^{(k+1)}$ and the gradients $\underline{\boldsymbol{g}}^{(k+1)}$ in each grain via Newton-Raphson iterations. The coupling is fully taken into account via a monolithic iteration scheme.

- "Local iteration loop": For given $\boldsymbol{F}(\boldsymbol{u}^{(k+1)})$, $\boldsymbol{g}^{(k+1)}$, solve the flow rule (Eq. (50)) for $\Delta\boldsymbol{\gamma}^{(k+1)}$ in each element via Newton-Raphson iterations.
- If convergence, then go to b.

b. If convergence, then go to 3.

3. If convergence, then set $k = k + 1$ and go to 1.

[a]Since the plastic slip is assumed to vanish on the grain boundaries, we only solve for the mechanical displacements during this loop.

7. Numerical example

In this section the behavior of the proposed model is studied by means of simple but effective numerical examples. The approach can be applied to single crystals as well as polycrystals. In the following, we investigate the hardening behavior of a specimen with side length L and comprising four grains. The length L is varied during the simulations in order to illustrate the grain size dependence of the hardening behavior of the crystal. The deformation of the grain structure is controlled by linearly varying displace-

ments at the boundaries to obtain macroscopic simple shear with a constant loading rate $\dot{\bar{\gamma}} = 0.01$ [1/s]. Plain strain is assumed. A total of 100 time steps have been used. The finite element meshes of the grain structures used in the numerical examples are generated by Voronoi polygonization and are depicted in Figure 1. The meshes are refined near the grain boundaries. The set of material parameters used in the examples are summarized in Table 1.

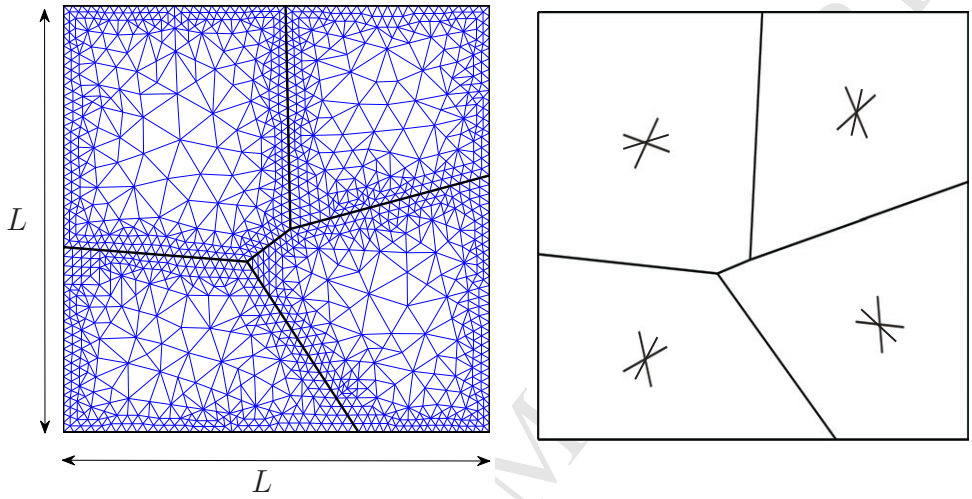

Figure 1: Left: Discretization and grain geometry used during simulations. The square grain structure consists of four grains and the thick black lines represent the grain boundaries. The grains are discretized with 726 (upper left grain), 620 (upper right), 630 (lower left), and 614 (lower right) elements, respectively. The mesh is refined near the grain boundaries. The side length L of the grain structure is varied during simulations in order to capture the size effects. A simple shear test as well as a tension test are performed. Right: Schematic sketch of slip plane directions $\boldsymbol{s}_\alpha$. Triple slip is assumed and slip plane directions are randomly distributed. In this example, the first slip planes read: 24.573° (lower left grain), 94.573° (lower right grain), 160.9° (upper left grain) and 35.845° (upper right grain). The second and the third slip plane vary by 30° respectively 60°.

As a first step, the macroscopic stress-strain response depicted in Figure 2 is discussed. The curves are plotted for different values of the side length L. On the left the stress-strain curve for the model with a non-zero dissipative length scale ($l_{d(\alpha)} \neq 0$) is depicted. As the length L decreases, the material response is stiffer in both cases, as expected. The size-dependence of the stress-strain response is due the existence of the slip gradient $\nabla\gamma_\alpha$ in the defect energy density (Eq. (17)) and, as a consequence, its existence in the

Parameter	Symbol	Value	
Young's modulus	E	$2 \cdot 10^5$	[MPa]
Poisson's ratio	ν	0.3	
local hardening modulus	H_α^l	200	[MPa]
gradient hardening modulus	H_α^g	$2.5 \cdot 10^4$	[MPa]
internal length scale	l_α	1	[μm]
initial yield stress	Y_α	750	[MPa]
relaxation time	t_*	10^4	[s]
drag stress	C_0	1	[MPa]
rate sensitivity parameter	m	1	

Table 1: Material parameters used

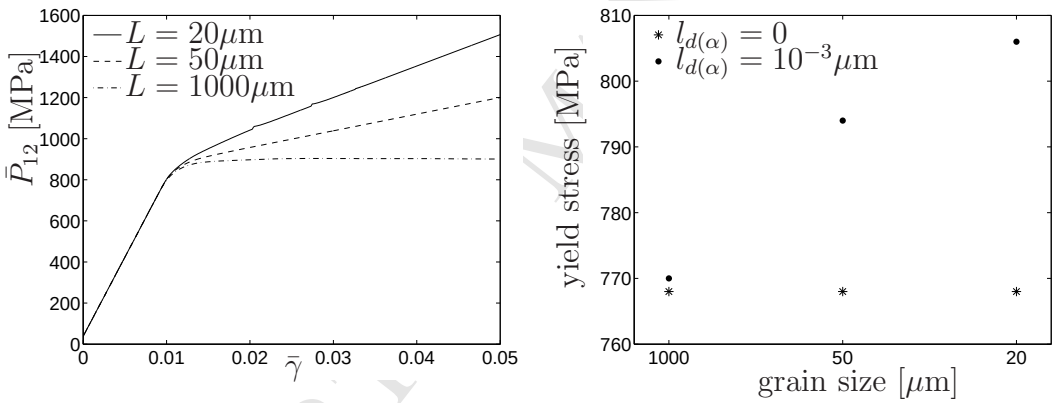

Figure 2: Simple shear test, four-grain structure.
Left: macroscopic stress-strain response ($\bar{P}_{12}$ vs. $\bar{\gamma}$); including dissipative strengthening ($l_{d(\alpha)} = 10^{-3}\,\mu$m)
Right: initial yield limit vs. grain size L. In case of a non-zero dissipative microforce $\boldsymbol{\xi}^{\text{dis}}$ the grain size influences the yield strength. $\star$: Dissipative length scale ($l_{d(\alpha)} = 0$) neglected. $\bullet$: Dissipative length scale ($l_{d(\alpha)} = 10^{-3}\,\mu$m) included.

governing equations. Moreover, the proposed model is capable of modeling a size-dependent yield stress if dissipative strengthening is included. The distribution of effective strain as well as of the dislocation density $\rho_{\text{GND,eff}} = \sqrt{\sum_\alpha [\nabla\gamma_\alpha \cdot \boldsymbol{s}_\alpha]^2}$ are plotted in Figs. 3 and 4 respectively.

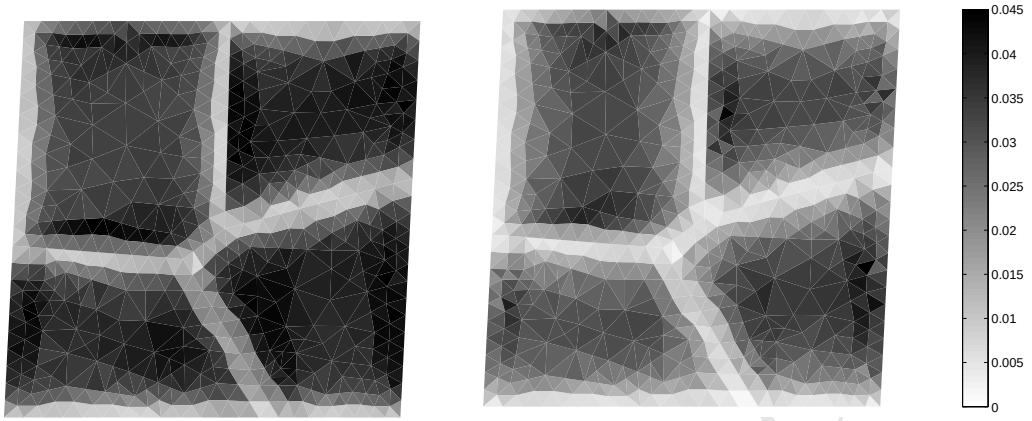

Figure 3: The effective strain $\Gamma_{\text{eff}} := \sqrt{\sum_\alpha |\Gamma_\alpha|^2}$ is plotted for a simple shear test; $l_{d(\alpha)} = 10^{-3}\ \mu$m at $\bar{\gamma} = 0.05$. The solutions for grain-structure side lengths $L = 20\ \mu$m (left) and $L = 50\ \mu$m (right) are shown. The difference in the distribution of the effective strain can clearly be seen.

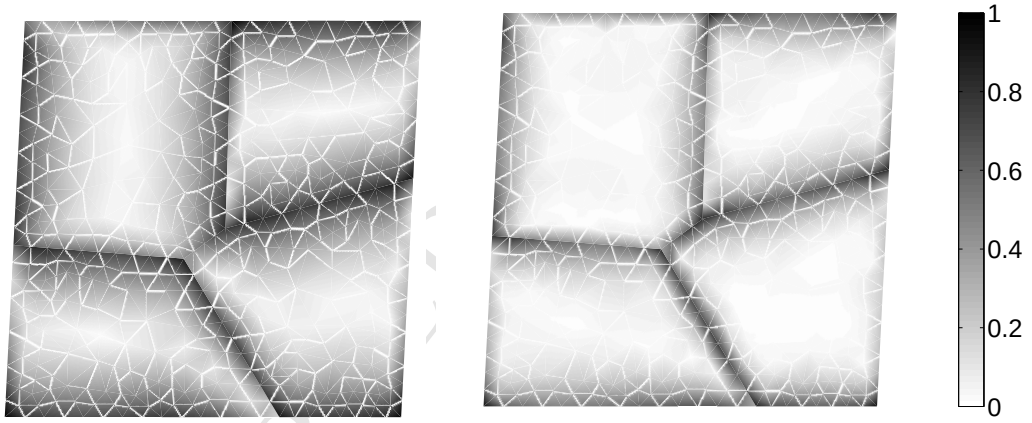

Figure 4: The effective dislocation density $\rho_{\text{GND,eff}} = \sqrt{\sum_\alpha [\nabla\gamma_\alpha \cdot \boldsymbol{s}_\alpha]^2}$ with unit $[\mu\text{m}^{-2}]$ is plotted for a simple shear test; $l_{d(\alpha)} = 10^{-3}\ \mu$m at $\bar{\gamma} = 0.05$. The solutions for grain-structure side lengths $L = 20\ \mu$m (left) and $L = 50\ \mu$m (right) are shown. The pile-up of dislocation densities at the grain boundaries is evident in the figures.

The model captures purely elastic response in line with the elastic-viscoplastic nature of the flow law. With an initial yield stress of $Y_\alpha = 750$ [MPa] the stress-strain response is initially linear elastic. At approximately $\bar{\gamma} = 0.01$ plastic behavior in the polycrystal with hardening becomes apparent.

For a zero dissipative length scale ($l_{d(\alpha)} = 0$) and non-zero energetic length

scale ($l_\alpha \neq 0$), size-dependent hardening is modeled. However, there is no real size-dependence in the initial yield limit. This is not in agreement with the experimental data which clearly show that the Hall–Petch effect ([46, 47]) goes along with a yield stress depending on the grain size. This drawback is overcome by including effects related to the slip rate gradients into the theory (and with it a non-zero dissipative material length scale). The computations are characterized by a sensitivity of the convergence behavior on the element level to the magnitude of $l_{d(\alpha)}$, see also the comments in [41, 29, 31, 32]. This limits the dissipative material length scale to $l_{d(\alpha)} = 10^{-3}$ μm in the computations presented in this section.

Not surprisingly, there is a direct dependence of yield stress and dissipative length scale. This is not easily discernible in Figures 2 (left), 5 (left) and 10 (left) and this effect is therefore presented in an alternative way in Figures 2 (right), 5 (right) and 10 (right) where the effect of $l_{d(\alpha)}$ is clear.

In addition, a computational tension test is performed with the four-grain structure. The stress-strain response is shown in Figure 5. Here, the von Mises stress $\bar{\sigma}$ is defined by

$$\bar{\sigma} = \sqrt{\tfrac{3}{2}\boldsymbol{\sigma}_{\mathrm{d}} : \boldsymbol{\sigma}_{\mathrm{d}}} \qquad \text{with } \boldsymbol{\sigma}_{\mathrm{d}} = \boldsymbol{\sigma} - \tfrac{1}{3}\mathrm{tr}\boldsymbol{\sigma}\boldsymbol{I}, \tag{55}$$

where $\boldsymbol{\sigma}$ is the Cauchy stress and (like the Piola–Kirchhoff stress component $\bar{P}_{12}$) is volume-averaged over the entire sample. Further, the effective generalized strain $\Gamma_{\mathrm{eff}} := \sqrt{\sum_\alpha |\Gamma_\alpha|^2}$ is illustrated in Figure 6 and the effective dislocation density $\rho_{\mathrm{GND,eff}}$ in Figure 7. In accordance with the experimental findings of Hall [46] and Petch [47], stiffer response in the hardening regime can be seen for smaller grain size, see Figure 5. Moreover, the dislocation density state of the GNDs as measured by the effective form $\rho_{\mathrm{GND,eff}}$ is larger near the grain boundaries and negligible in the interior (cf. Figure 7 for the simulation results and e.g. Kocks [48] for experimental data). The distribution in general and the order of the value of the GND density measure corresponds well with the tension test performed by [18]. The existence of GNDs is usually assumed due to lattice orientation mismatch between neighboring grains - as is the case in our polycrystalline grain structure.

The second example is that of a 25-grain structure, shown in Figure 8. Again, random triple slip is assumed in each grain. The macroscopic stress-strain response for simple shear test is shown in Figure 9 while Figure 10 illustrates the distribution of the generalized strain inside the grain structure at $\bar{\gamma} = 0.05$ for side lengths $L = 20\mu$m and $L = 50\mu$m, and for the case

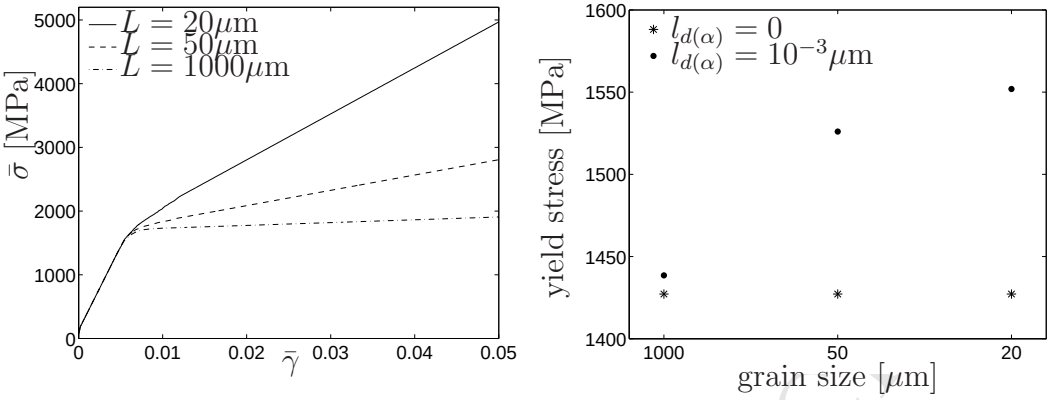

Figure 5: Tension test, four-grain structure.
Left: macroscopic stress-strain response ($\bar{\sigma}$ vs. $\bar{\gamma}$), dissipative length scale ($l_{d(\alpha)} = 10^{-3}\,\mu$m) included.
Right: initial yield limit vs. grain size L. For a purely energetic theory the yield stress is not size dependent, whereas for a non-zero dissipative microforce $\boldsymbol{\xi}^{\text{dis}}$ a dependence on the specimen size L can clearly be seen. The smaller the size of the specimen, the larger the yield stress. $\star$: Dissipative length scale ($l_{d(\alpha)} = 0$) neglected. $\bullet$: Dissipative length scale ($l_{d(\alpha)} = 10^{-3}\,\mu$m) included.

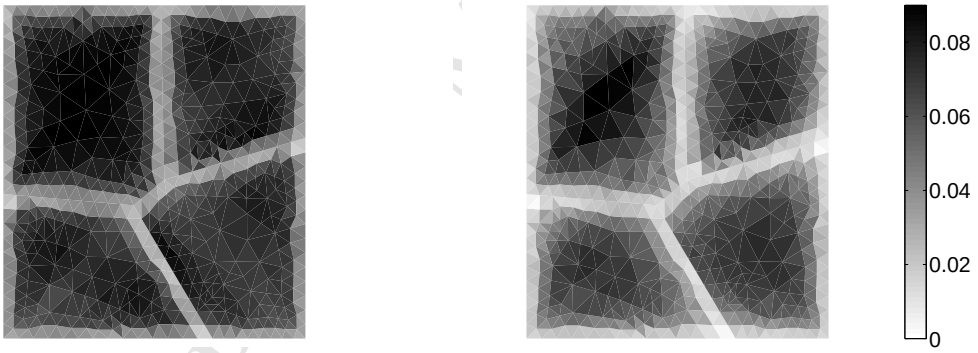

Figure 6: Tension test; $l_{d(\alpha)} = 10^{-3}$ μm. The effective generalized strain Γ_{eff} is shown for grain-structure side lengths $L = 20$ μm (left) and $L = 50$ μm (right) at $\bar{\gamma} = 0.05$. The difference in the distribution of the effective strain can clearly be seen.

of dissipative strengthening ($l_{d(\alpha)} = 10^{-4}\,\mu$m). In comparison to the 4-grain example, the size-effect is more profound. The numerical simple shear test is performed for the same material, i.e. the same material parameters. For large specimen, the stress-strain response shows a behavior which is approximately as stiff for the 25-grain structure as for the 4-grain example. The 25-grain

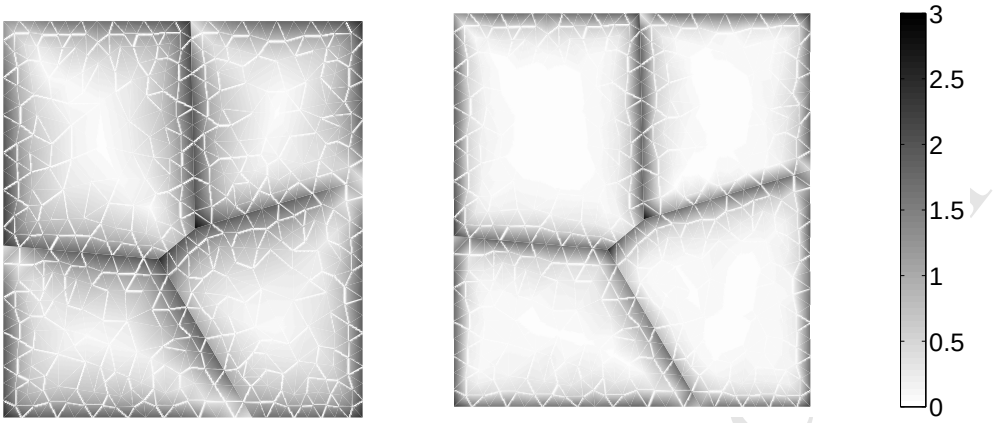

Figure 7: Tension test; $l_{d(\alpha)} = 10^{-3}$ μm. The effective dislocation density $\rho_{\text{GND, eff}}$ with unit $[\mu\text{m}^{-2}]$ is shown for grain-structure side lengths $L = 20$ μm (left) and $L = 50$ μm (right) at $\bar{\gamma} = 0.05$. As the sample size decreases, the GND density increases.

polycrystal allows for a lot of grain interaction because of the larger amount of grains. This leads to significantly larger influence of the size-effect. In other words, a specimen of length $L = 20$ μm consisting of 25 grains responds stiffer than a specimen of the same size consisting of 4 grains - in accordance to the Hall–Petch effect.

It is assumed that the dislocation motion is blocked at the grain boundaries which is realized by assuming micro-hard boundary conditions. Thus, the plastic slip γ_α vanishes there. The non-uniformity of the plastic deformation is due to the dislocation pile-up which results from the slip being blocked at the grain boundaries. The boundary layer thickness increases, and the deformation inhomogeneity becomes more pronounced, as the length L decreases. The effective generalized strain is illustrated in Figure 10.

8. Discussion and concluding remarks

A strain gradient theory of plasticity incorporating dissipative microstresses has been presented. The theory is viscoplastic and follows closely the model due to Gurtin and co-authors [30, 11], but differs from these and other treatments in that a viscoplastic regularization of Perzyna type is used. In particular provision is made for an elastic range followed by viscoplastic flow. The link to the approach by Ekh et al. [8] is made clear. It is noted that the energetic theory of Gurtin [11] and the theory due to Ekh et al. [8] (which

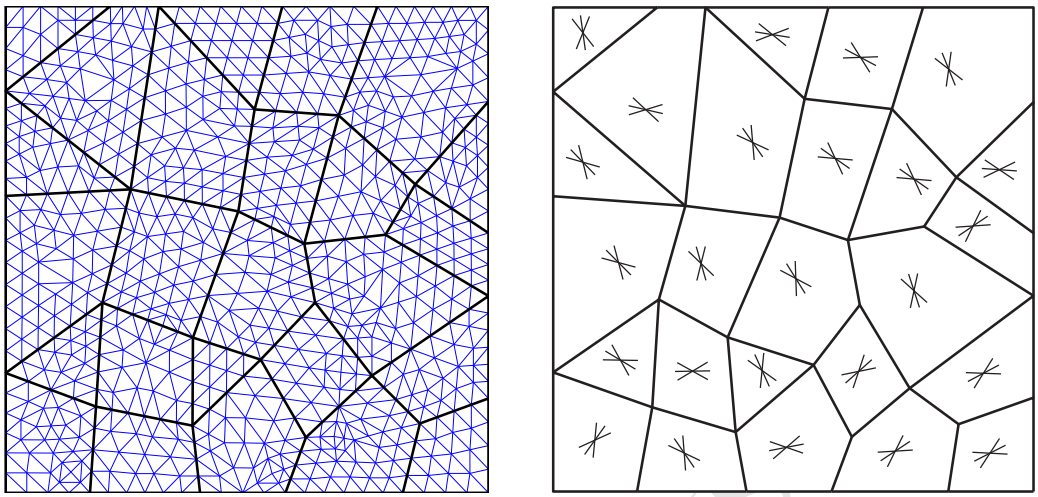

Figure 8: Left: Discretization and grain geometry of the 25-grain-structure used during simulations. A simple shear test is performed.
Right: Schematic sketch of slip plane directions $\boldsymbol{s}_\alpha$. Triple slip is assumed and slip plane directions are randomly distributed.

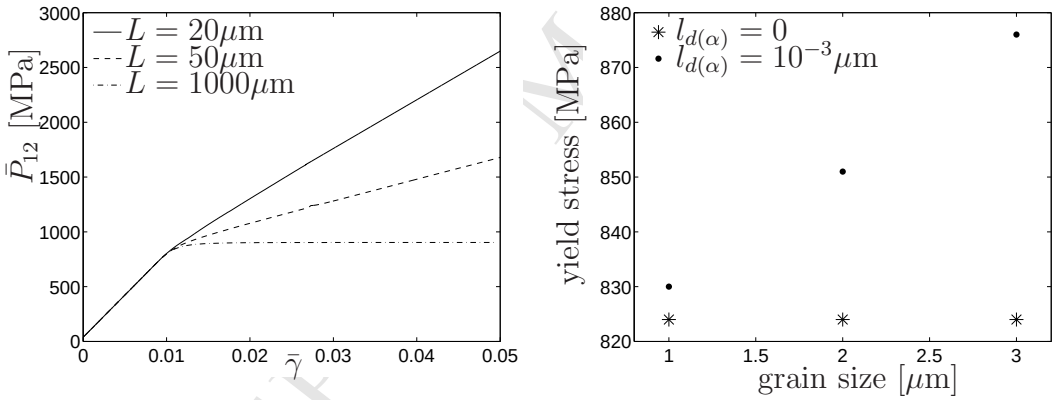

Figure 9: 25 grain structure, simple shear. Macroscopic stress–strain response ($\bar{P}_{12}$ vs. $\bar{\gamma}$) showing the size dependence on the amount of hardening and the effect of dissipative strengthening.
Right: initial yield limit vs. grain size L. In case of a non-zero dissipative microforce $\boldsymbol{\xi}^{\mathrm{dis}}$ the grain size influences the yield strength. $\star$: Dissipative length scale ($l_{d(\alpha)} = 0$) neglected. $\bullet$: Dissipative length scale ($l_{d(\alpha)} = 10^{-4}\,\mu$m) included.

is purely energetic) are equivalent. In contrast to most approaches, strain gradients enter the model presented in this contribution via the free energy Ψ and, additionally, via the dissipative microforce $\boldsymbol{\xi}^{\mathrm{dis}}_\alpha$. The dissipative harden-

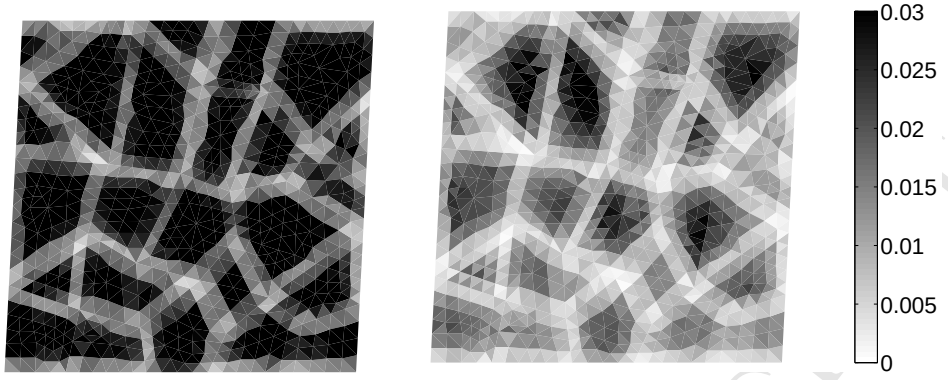

Figure 10: Effective strain Γ_{eff} for $l_{d(\alpha)} = 10^{-4}$ μm. The solutions for grain-structure side lengths $L = 20$ μm (left) and $L = 50$ μm (right) are depicted for the 25-grain-polycrystal at $\bar{\gamma} = 0.05$. Computations are carried out for monotonic loading with a maximum macroscopic shear deformation $\bar{\gamma}_{\max} = 0.05$.

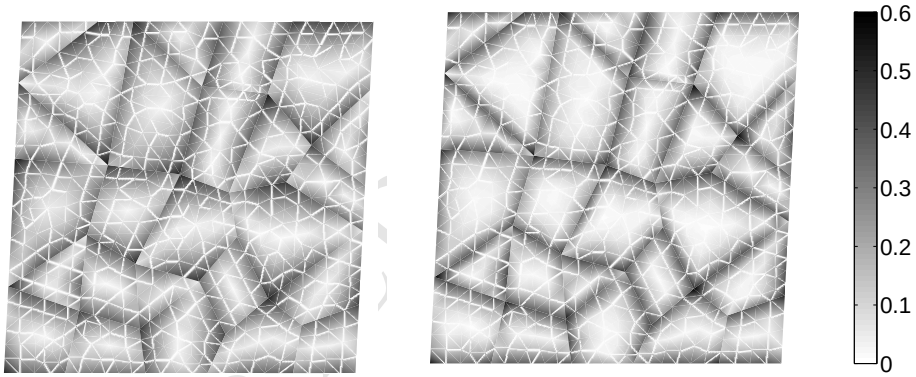

Figure 11: Effective dislocation density $\rho_{\text{GND, eff}}$ (with unit $[\mu\text{m}^{-2}]$) for $l_{d(\alpha)} = 10^{-4}$ μm. The solutions for grain-structure side lengths $L = 20$ μm (left) and $L = 50$ μm (right) are depicted for the 25-grain-polycrystal at $\bar{\gamma} = 0.05$. Computations are carried out for monotonic loading with a maximum macroscopic shear deformation $\bar{\gamma}_{\max} = 0.05$.

ing associated with the term $\text{Div}\boldsymbol{\xi}_\alpha^{\text{dis}}$ results in a size-dependent yield stress. The energetic theory of Ekh et al. [8] has been extended by inclusion of the vector dissipative microstress. This leads inter alia to a size-dependent yield

stress.

Dissipative hardening in polycrystals has hardly been studied. While there are some works in which it forms part of the theory, the physical interpretation of the dissipative length scale has not been investigated in great detail. To the best of the authors' knowledge, the work by Lele and Anand [31] is the only one containing numerical results for a model with a dissipative length scale. Voyiadjis and Deliktas [40] investigate the size effect due to the dissipative length scale for the example of a thin film on thick substrates. Bardella and Giacomini [28] present closed-form solutions for a small example by exploitation of a Γ-convergence technique. Further, they prove that in their approach the absence of a dissipative length scale may lead to non-unique solutions in the case of perfect plasticity.

Energetic material length scales have a direct physical link to the density of geometrically necessary dislocations via the length of the Burgers vector. However, the precise interpretation of this length scale across the wide range of theories is not completely established. Unfortunately, the situation is even less clear for the dissipative material length scale. Nevertheless, the necessity of its introduction into continuum mechanics theories for extended crystal plasticity is already acknowledged by many researchers.

The algorithm presented and implemented is an extension of that due to Ekh et al. [8] in that it employs a dual-mixed approach. The algorithm used here differs in a significant respect, however, in that provision has to be made for the additional variable in the form of the dissipative microstress. In the results presented here it is found that the energetic scheme ($l_{d(\alpha)} = 0$) is more robust than the dissipative one ($l_{d(\alpha)} \neq 0$), in the sense that convergence is only achieved for values of $l_{d(\alpha)}$ up to a certain magnitude. Further, it has been noted that the manner in which the local governing equation (50) is used is a delicate matter: whereas the code runs smoothly if Eq. (50) is multiplied throughout by the denominator, difficulties ensue if Eq. (50) is implemented as written. Note that Lele and Anand [31] also report that their model "possesses a mathematically attractive structure, our experience with numerical experiments which use these constitutive equations is that they are too tightly coupled". Nevertheless, the model and simulations presented in this work provide additional useful insights into the behavior of gradient theories which include both energetic and dissipative material lengths scales. Further, the extension to dissipative effects is derived consistently via thermodynamic considerations rather than proposing it in an ad hoc fashion.

Recent and current research on dissipative stresses and length scales in

extended crystal plasticity theories clearly points out the need to set up gradient theories with more than one material length scale in order to improve the mapping of strengthening and hardening mechanisms in (poly-)crystals. The work presented in this paper contributes to this ongoing research direction, suggesting a way on how to incorporate dissipative microstress (and with it a dissipative length scale) as an additional variable, together with a corresponding additional flow equation. However, as also stated by the aforementioned authors, more attention and work needs to be done in this direction in order to be able to accurately describe the material behavior.

Acknowledgements. This research was done while S.B. visited the Centre for Research in Computational and Applied Mechanics, University of Cape Town, whose hospitality is gratefully acknowledged. Her stay was supported by the Heinrich Hertz foundation (Düsseldorf, Germany) which is also gratefully acknowledged.
The work of B.D.R. was supported through the South African Research Chair in Computational Mechanics by the Department of Science and Technology and the National Research Foundation. This support is gratefully acknowledged. The authors are very grateful to the scientific editor and to the anonymous referees for their helpful comments and suggestions leading to the improvement of this contribution.

References

[1] H. E. Tresca, Mémoires sur l'Ecoulement des Corps Solides, Mém. Sav. Acad. Sci., Paris, (Science Mathématiques et Physiques) 10 (1872) 75–135.

[2] J. C. Simo, T. J. R. Hughes, Computational Inelasticity, Vol. 7, Springer, 1998.

[3] J. C. Simo, Topics on the numerical analysis and simulation of plasticity, in: P. G. Ciarlet, J. L. Lions (Eds.), Handbook of Numerical Analysis, Vol. VI of Handbook of numerical analysis, North-Holland, Amsterdam, 1998, pp. 183–499.

[4] E. C. Aifantis, On the microstructural origin of certain inelastic models, Journal of Engineering Materials and Technology 106 (1984) 326–330.

[5] A. Acharya, J. L. Bassani, A. Beaudoin, Geometrically necessary dislocations, hardening, and a simple gradient theory of crystal plasticity, Scripta Materialia 48 (2003) 167–172.

[6] J. L. Bassani, Incompatibility and a simple gradient theory of plasticity, Journal of the Mechanics and Physics of Solids 49 (2001) 1983–1996.

[7] U. Borg, A strain gradient crystal plasticity analysis of grain size effects in polycrystals, European Journal of Mechanics A/Solids 26 (2007) 313–324.

[8] M. Ekh, M. Grymer, K. Runesson, T. Svedberg, Gradient crystal plasticity as part of the computational modeling of polycrystals, International Journal for Numerical Methods in Engineering 72 (2007) 197–220.

[9] L. P. Evers, W. A. M. Brekelmans, M. G. D. Geers, Scale dependent crystal plasticity framework with dislocation density and grain boundary effects, International Journal of Solids and Structures 41 (2004) 5209–5230.

[10] M. E. Gurtin, On the plasticity of single crystals: free energy, microforces, plastic-strain gradients, Journal of the Mechanics and Physics of Solids 48 (2000) 989–1036.

[11] M. E. Gurtin, A theory of grain boundaries that accounts automatically for grain misorientation and grain-boundary orientation, Journal of the Mechanics and Physics of Solids 56 (2008) 640–662.

[12] M. E. Gurtin, L. Anand, A theory of strain-gradient plasticity for isotropic, plastically irrotational materials. Part I: Small deformations, Journal of the Mechanics and Physics of Solids 53 (2005) 1624–1649.

[13] C.-S. Han, H. Gao, Y. Huang, W. Nix, Mechanism-based strain gradient crystal plasticity-I. Theory, Journal of the Mechanics and Physics of Solids 53 (2005) 1188–1203.

[14] M. Kuroda, V. Tvergaard, On the formulations of higher-order strain gradient crystal plasticity models, Journal of the Mechanics and Physics of Solids 56 (2008) 1591–1608.

[15] N. Ohno, D. Okumura, Higher-order stress and grain size effects due to self-energy of geometrically necessary dislocations, Journal of the Mechanics and Physics of Solids 55 (2007) 1879–1898.

[16] P. Gudmundson, A unified treatment of strain gradient plasticity, Journal of the Mechanics and Physics of Solids 52 (2004) 1379–1406.

[17] S. Bargmann, B. Svendsen, M. Ekh, An extended crystal plasticity model for latent hardening in polycrystals, submitted.

[18] L. P. Evers, W. A. M. Brekelmanns, M. G. D. Geers, Non-local crystal plasticity model with intrinsic ssd and gnd effects, Journal of the Mechanics and Physics of Solids 52 (2004) 2379–2401.

[19] M. E. Gurtin, A theory of viscoplasticity that accounts for geometrically necessary dislocations, Journal of the Mechanics and Physics of Solids 50 (2002) 5–32.

[20] M. Kuroda, V. Tvergaard, Studies of scale dependent crystal viscoplasticity models, Journal of the Mechanics and Physics of Solids 54 (2006) 1789–1810.

[21] R. de Borst, H.-S. Mühlhaus, Gradient-dependent plasticity: formulation and algorithmic aspects, International Journal for Numerical Methods in Engineering (1992) 521–539.

[22] J. K. Djoko, F. Ebobisse, A. T. McBride, B. D. Reddy, A discontinuous Galerkin formulation for classical and gradient plasticity. Part 1: Formulation and analysis, Computer Methods in Applied Mechanics and Engineering 196 (2007) 3881–3897.

[23] J. K. Djoko, F. Ebobisse, A. T. McBride, B. D. Reddy, A discontinuous Galerkin formulation for classical and gradient plasticity. Part 2: Algorithms and numerical analysis, Computer Methods in Applied Mechanics and Engineering 197 (2007) 1–21.

[24] T. Liebe, P. Steinmann, Theory and numerics of a thermodynamically consistent framework for geometrically linear gradient plasticity, International Journal for Numerical Methods in Engineering 51 (2001) 1437–1467.

[25] E. Bittencourt, A. Needleman, M. E. Gurtin, E. Van der Giessen, A comparison of nonlocal continuum and discrete dislocation plasticity predictions, Journal of the Mechanics and Physics of Solids 51 (2003) 281–310.

[26] T. Svedberg, K. Runesson, An algorithm for gradient-regularized plasticity coupled to damage based on a dual mixed FE-formulation, Computer Methods for Applied Mechanics and Engineering 161 (1998) 49–65.

[27] L. Anand, M. E. Gurtin, S. P. Lele, C. Gething, A one-dimensional theory of strain-gradient plasticity: Formulation, analysis, numerical results, Journal of the Mechanics and Physics of Solids 53 (2005) 1789–1826.

[28] L. Bardella, A. Giacomini, Influence of material parameters and crystallography on the size effects describable by means of strain gradient plasticity, Journal of the Mechanics and Physics of Solids 56 (2008) 2906–2934.

[29] N. A. Fleck, J. W. Hutchinson, A reformulation of strain gradient plasticity, Journal of the Mechanics and Physics of Solids 49 (2001) 2245–2271.

[30] M. E. Gurtin, A gradient theory of small–deformation isotropic plasticity that accounts for the Burgers vector and for dissipation due to plastic spin, Journal of the Mechanics and Physics of Solids 52 (2004) 2545–2568.

[31] S. P. Lele, L. Anand, A small-deformation strain-gradient theory for isotropic viscoplastic materials, Philosophical Magazine 88 (2008) 3655–3689.

[32] S. P. Lele, L. Anand, A large-deformation strain-gradient theory for isotropic viscoplastic materials, International Journal of Plasticity 25 (2009) 420–453.

[33] C. F. Niordson, B. N. Legarth, Strain gradient effects on cyclic plasticityg, Journal of the Mechanics and Physics of Solids 58 (2010) 542–557.

[34] A. Evans, J. Hutchinson, A critical assessment of theories of strain gradient plasticity, Acta Materialia 57 (2004) 1675–1688.

[35] W. Nix, H. Gao, Indentation size effects in crystalline materials: a law for strain gradient plasticity, Journal of the Mechanics and Physics of Solids 46 (1998) 411–425.

[36] I. Ertürk, J. A. W. van Dommelen, M. G. D. Geers, Energetic dislocation interactions and thermodynamical aspects of strain gradient crystal plasticity theories, Journal of the Mechanics and Physics of Solids 57 (2009) 1801–1814.

[37] B. D. Reddy, The role of dissipation and defect energy in variational formulations of problems in strain-gradient plasticity. Part 2: Single-crystal plasticity, Continuum Mechanics and Thermodynamics, in review.

[38] J. Rice, Inelastic constitutive relations for solids: an internal-variable theory and its application to metal plasticity, Journal of the Mechanics and Physics of Solids 19 (1971) 433–455.

[39] M. Ekh, S. Bargmann, M. Grymer, Influence of grain boundary conditions on modeling of size-dependence in polycrystals, Acta Mechanica 218 (2011) 103–113.

[40] G. Z. Voyiadjis, B. Beliktas, Mechanics of strain gradient plasticity with particular reference to decomposition of the state variables into energetic and dissipative components, International Journal of Engineering Science 47 (2009) 1405–1423.

[41] S. Bargmann, M. Ekh, K. Runesson, B. Svendsen, Modeling of polycrystals with gradient crystal plasticity: A comparison of strategies, Philosophical Magazine 90 (2010) 1263–1288.

[42] M. E. Gurtin, B. D. Reddy, Alternative formulations of isotropic hardening for Mises materials, and associated variational inequalities, Continuum Mechanics and Thermodynamics 21 (2009) 237–250.

[43] P. Fredriksson, P. Gudmundson, Size-dependent yield strength of thin films, International Journal of Plasticity 21 (2005) 1834–1854.

[44] S. Yefimov, I. Groma, E. van der Giessen, A comparison of a statistical-mechanics based plasticity model with discrete dislocation plasticity calculations, Journal of the Mechanics and Physics of Solids 52 (2004) 279–300.

[45] M. E. Gurtin, A. Needleman, Boundary conditions in small-deformation, single-crystal plasticity that account for the Burgers vector, Journal of the Mechanics and Physics of Solids 53 (2005) 1–31.

[46] E. O. Hall, The deformation and ageing of mild steel: III discussion of results, Proceedings Physical Society London B 64 (1951) 747–753.

[47] N. J. Petch, The cleavage strength of polycrystals. I, Journal of Iron and Steel Institute 174 (1953) 25–28.

[48] U. F. Kocks, The relation between polycrystal deformation and single crystal deformation, Metallurgical Transactions 1 (1970) 1121–1144.